

# Con ned Coulomb system s w ith absorbing boundaries: the two-dim ensional two-com ponent plasma

Lina M erchan and Gabriel Tellez<sup>y</sup>

D epartamento de F sica, Universidad de Los Andes, A A . 4976, Bogota, Colombia

Using a solvable model, the two-dim ensional two-com ponent plasma, we study a Coulomb gas con ned in a disk and in an annulus w ith boundaries that can absorb some of the negative particles of the system . We obtain explicit analytic expressions for the grand potential, the pressure and the density pro les of the system . By studying the behavior of the disjoining pressure we nd that w ithout the absorbing boundaries the system is naturally unstable, while w ith attractive boundaries the system is stable. The results for the density pro les show the formation of a positive layer near the boundary that screens the absorbed negative particles, a typical behavior in charged systems. We also compute the absorbed charge on the boundary and show that it satis es a certain number of relations, in particular a electro-neutrality sum rule.

**K ey words:** Coulomb system s, two-com ponent plasma, absorbing boundaries, soap lm s and bubbles, m ielles and vesicles, disjoining pressure, charge density

## I. INTRODUCTION

In this paper we study the classical (ie. non-quantum) equilibrium statistical mechanics properties of con ned Coulomb system s w ith absorbing boundaries. A Coulomb system is a system of charged particles interacting through the Coulomb potential. There are several interesting realizations of Coulomb system s w ith several applications such as plasma s, electrolytes, colloidal suspensions, etc... In the present paper we are interested in the case where the Coulomb system is con ned w ith boundaries that can attract and absorb some particles of the system . Our study of this kind of system s will be done using a solvable model of Coulomb system : the symmetric two-dim ensional two-com ponent plasma, a system of two kind of oppositely charged particles  $q$  at thermal equilibrium at an inverse temperature  $\beta = (k_B T)^{-1}$ . The classical equilibrium statistical mechanics of the system can be exactly solved when  $q^2 = 2$ .

One can think of several examples where the present situation of Coulomb system s con ned w ith absorbing boundaries is relevant, for instance in a plasma or an electrolyte near an electrode w ith absorbing sites [1, 2]. Another situation in which we will focus our attention is in solutions of amphiphilic molecules and ions for example in soap lm s and bubbles. Amphiphilic molecules have an hydrophobic tail and an hydrophilic charged head (usually negative) and, for this reason, when they are submerged in water they rearrange them selves in such a way as to minimize the contact of the hydrophobic tails w ith the surrounding medium. They can achieve configurations such as bilayers, m ielles and vesicles, among others.

In a previous paper [3] we studied a soap lm by modeling it as a Coulomb system con ned in a slab. A soap lm

can be seen as a system of amphiphilic molecules in a bilayer con guration w ith a water inner layer. The overall neutral system w ith negatively charged amphiphilic anions and positive micro-cations (usually  $\text{Na}^+$ ) in water was modeled as a two-dim ensional two-com ponent plasma. The two dimensions were in the breadth of the lm not on the surface: we studied a cross section of the lm . Because of the hydrophobicity of their tails, the soap anions prefer to be in the boundaries of the lm . This was modeled by a one-body attractive short-range external potential acting over them . This means that the negative particles felt an attractive potential over a small distance near each boundary. In this sense the negative particles of the system can be "absorbed" by the boundary.

In Ref. [3] we found exact expressions for the density, correlations and pressure inside the lm . By studying the disjoining pressure, we were able to conclude that the Coulomb interaction plays an important role in the collapse of a thick soap lm to a much thinner lm . Actually if a large number of amphiphilic molecules are in the boundary due to a large strength of the attractive external potential near the boundary, the system is always stable. On the other hand if the attractive potential near the boundary is not strong enough a thick lm will not be stable and will collapse to a thin lm .

These results can be compared (qualitatively due to the simplicity of the model under consideration) to the experimental situation of the transition of a thick lm to a thin black lm . These black lm phenomena occur when the soap lm s width is smaller than visible light wavelength and it is seen black. Two types of black lm s are observed experimentally: the common black lm and the much thinner Newton black lm .

It is interesting to know to what extent the results of our previous work [3] depend on the geometry. Here we study this two-com ponent plasma system con ned in two other geometries, a disk and an annulus. As we mentioned before, amphiphilic molecules in water can achieve m ielles and vesicles among others con g-

<sup>x</sup>Electronic address: lmercha@uniandes.edu.co

<sup>y</sup>Electronic address: gtellez@uniandes.edu.co

urations. In two dimensions, a cylindrical cell can be seen as a disk and a cylindrical vesicle as an annulus. If the length of the cylindrical cell or vesicle is much larger than its radius it is reasonable to assume that the system is invariant in the longitudinal direction and so we study only a cross section of the system: a disk or an annulus. The Coulomb interaction is then the two-dimensional Coulomb potential which is  $v_c(r) = -\ln(r/d)$  for two particles at a distance  $r$  of each other. The length  $d$  is an arbitrary length which fixes the zero of the potential.

Two-dimensional Coulomb systems with long interaction have properties that are similar to those in three-dimensional charged systems with the usual  $1/r$  potential. They satisfy Gauss law and Poisson equation in two dimensions. Several universal properties, such as screening effects, are direct consequences of the harmonic nature of the  $-\ln(r/d)$  and  $1/r$  potentials, which are the solutions of the two- and three-dimensional Poisson equation. Therefore the exact solutions obtained for the 2D models play an important role in understanding real 3D Coulomb systems.

The rest of this work is organized as follows. In section II we present in detail the system under consideration and briefly review how this model can be exactly solved. In section III we compute the grand potential of the system and the disjoining pressure and study the stability of the system. In section IV we compute the density profiles of the different types of particles in the system and the absorbed charge on the boundaries. Finally, we conclude recalling the main results of the present work.

## II. THE MODEL AND METHOD OF SOLUTION

The system under consideration is a two-dimensional system composed of two types of point particles with charges  $q$ . Two particles with charges  $sq$  and  $s'q$  at a distance  $r$  apart interact with the two-dimensional Coulomb potential  $ss'q^2 \ln(r/d)$  where  $d$  is an arbitrary length. This system is known as the symmetric two-dimensional two-component plasma.

When the Boltzmann factor for the Coulomb potential is written, the dimensional Coulomb coupling constant appears:  $\epsilon = q^2 = k_B T = q^2$ . Notice that in two dimensions  $q^2$  has dimensions of energy. For a system of point particles if  $\epsilon < 2$  the system is unstable against the collapse of particles of opposite sign, the thermodynamics of the system are not well defined unless one considers hard-core particles or another regularization procedure (for instance a lattice model instead of a continuous gas). On the other hand, if  $\epsilon < 2$  the thermal agitation is enough to avoid the collapse and the system of point particles is well defined. The two-component plasma is known to be equivalent to the sine-Gordon model and using this relationship and the results known for this integrable field theory, the thermodynamic properties of the two-component plasma in the bulk have been exactly

determined [4] in the whole range of stability  $\epsilon < 2$ . However, there are no exact results for confined systems for arbitrary  $\epsilon$  (with the exception of a Coulomb system near an infinite plane conductor [5] or ideal dielectric [6] wall).

It is also well-known for some time that when  $\epsilon = 2$  the sine-Gordon field theory is at its free fermion point. This means that the system is equivalent to a free fermion field theory and therefore much more information on the system can be obtained. In particular the thermodynamic properties and correlation functions can be exactly computed even for confined systems in several different geometries and different boundary conditions [7, 8, 9, 10, 11, 12, 13, 14]. From now on we will consider only the case when  $\epsilon = 2$ .

Since at  $\epsilon = 2$  a system of point particles is not stable one should start with a regularized model with a cut-off distance  $a$  which can be the diameter of the hard-core particles or the lattice spacing in a lattice model [7]. The system is worked out in the grand-canonical ensemble at given chemical potentials  $\mu_+$  and  $\mu_-$  for the positive and negative particles respectively. In the limit of a continuous model  $a \rightarrow 0$  the grand partition function and the bulk densities diverge. However the correlation functions have a well-defined limit. In this continuous limit it is useful to work with the rescaled fugacities [9]  $m = 2 \epsilon = a^2$  that have inverse length dimensions. The length  $m^{-1}$  can be shown to be the screening length of the system [9]. If external potentials  $V(r)$  act on the particles (as in our case) it is useful to define position-dependent fugacities  $m(r) = m \exp(-V(r))$ .

Let us briefly review the method of resolution described by Jancovici and Cornu [8, 9] for the two-component plasma. It will be useful to use the complex coordinates  $z = re^{i\phi} = x + iy$  for the position of the particles. For a continuous model,  $a \rightarrow 0$ , ignoring the possible divergences for the time being, it is shown in Ref. [9] that the equivalence of the two-component plasma with a free fermion theory allows the grand partition function to be written as

$$= \det \begin{matrix} 0 & 2\theta_z & & & \\ & 0 & & & \\ & & 1 & & \\ & & & m_+(r) & 2\theta_z \\ & & & 2\theta_z & 0 \\ & & & & m_-(r) \end{matrix} \quad (2.1)$$

Then defining an operator  $K$  as

$$K = \begin{matrix} 0 & 2\theta_z & & & & \\ & 0 & & & & \\ & & 1 & & & \\ & & & m_+(r) & 0 & \\ & & & 2\theta_z & 0 & \\ & & & & 0 & m_-(r) \end{matrix} \quad (2.2)$$

the grand partition function can be expressed as

$$= \det(1 + K) : \quad (2.3)$$

The calculation of the grand potential  $\epsilon = \ln$  and the pressure  $p = \epsilon = \epsilon V$  where  $V$  is the volume (in a two-dimensional system this refers to the area), reduces to finding the eigenvalues of  $K$  because the grand potential can be written as

$$= k_B T \sum_i^X \ln(1 + \epsilon_i) \quad (2.4)$$

where  $\lambda$  are the eigenvalues of the operator  $K$ .

On the other hand, the calculation of the one-particle densities and correlations reduces to finding a special set of Green functions. As usual, the density can be expressed as a functional derivative

$$\langle r \rangle = m_+(r) \frac{h}{m_-(r)} \quad (2.5)$$

If we define the  $2 \times 2$  matrix

$$\begin{aligned} G(r_1; r_2) = & \begin{pmatrix} G_{++}(r_1; r_2) & G_+(r_1; r_2) \\ G_+(r_1; r_2) & G_-(r_1; r_2) \end{pmatrix} \end{aligned} \quad (2.6)$$

as the kernel of the inverse of the operator

$$\begin{pmatrix} m_+(r) & 2\theta_z \\ 2\theta_z & m_-(r) \end{pmatrix} \quad (2.7)$$

then the one-body density and two-body Ursell functions can be expressed in terms of these Green functions as

$$\begin{aligned} s_1(r_1) &= m_{s_1} G_{s_1 s_1}(r_1; r_1); \\ s_{12}^{(2)T}(r_1; r_2) &= m_{s_1} m_{s_2} G_{s_1 s_2}(r_1; r_2) G_{s_2 s_1}(r_2; r_1) \end{aligned} \quad (2.8)$$

where  $s_{1,2} \in \{+, -\}$  denote the sign of the particles. In polar coordinates these Green functions satisfy the following set of equations

$$\begin{aligned} 2 & \frac{h}{4} \frac{m_+(r_1)}{e^{i\theta_{r_1}}} = \frac{h}{4} \frac{e^{i\theta_{r_1}}}{m_-(r_1)} \frac{\frac{i\theta_{r_1}}{r_1} - \frac{i}{3}}{e^{i\theta_{r_1}} + \frac{i\theta_{r_1}}{r_1}} G(r_1; r_2) I \end{aligned} \quad (2.9)$$

with  $I$  being the unit  $2 \times 2$  matrix.

The above formalism is very general, it can be applied to a variety of situations. In the case we are interested in, we will consider two geometries in which the system is confined: a disk of radius  $R$  and an annulus of inner and outer radius  $R_1$  and  $R_2$  respectively.

The negative particles are supposed to model amorphous molecules and therefore they are attracted to the boundaries of the system while positive particles are not. This is modeled by an attractive external one-body potential  $V(r)$  acting on the negative particles near the boundary while for the positive particles  $V_+(r) = 0$ .

Actually we will consider two models for this potential. In the first model (Model I) the fugacity  $m_-(r)$  for the negative particles reads, for the disk geometry,

$$m_-(r) = m e^{-V(r)} = m_+(r - R) \quad (2.10)$$

inside the disk, while  $m_+ = m$  is constant. Outside the disk  $r > R$  both fugacities vanish. In the annulus geometry,

$$m_-(r) = m_+ + \lambda_1(r - R_1) + \lambda_2(r - R_2) \quad (2.11)$$

inside the annulus. The coefficients  $\lambda_1$  and  $\lambda_2$  measure the strength of the attraction to the walls. In the following we will call these coefficients adhesivities.

In the second model (Model II) that we will eventually consider the external potential  $V(r)$  is a step function with a range  $\Delta$  of attraction near the boundary. This model allows us to obtain valuable information regarding the frontier regions. Actually we will report here only the main results for the annulus geometry with model II in the section IV C, further results on this model on the disk geometry can be found in Ref. [15].

In the annulus geometry, there are two outer regions, each one has a width  $\Delta$ , and an inner region that has a thickness  $R_2 - R_1 - 2\Delta$ . We can distinguish three regions for the annulus geometry: the inner border  $R_1 < r_1 < R_1 + \Delta$  (region 1), the bulk of the  $R_1 + \Delta < r_1 < R_2$  (region 2) and the outer border  $R_2 - \Delta < r_1 < R_2$  (region 3). So for this model in the annulus geometry, we define the position dependent fugacities as

$$\begin{aligned} m_+(r_1) &= \begin{cases} m & \text{if } r_1 < R_1 \\ \frac{m}{2} & \text{if } R_1 \leq r_1 < R_1 + \Delta \\ \frac{m}{2} & \text{if } R_1 + \Delta \leq r_1 < R_2 \\ m & \text{if } R_2 \leq r_1 \end{cases} \end{aligned} \quad (2.12a)$$

$$\begin{aligned} m_-(r_1) &= \begin{cases} m & \text{if } r_1 < R_1 \\ \frac{m}{2} & \text{if } R_1 \leq r_1 < R_1 + \Delta \\ \frac{m}{2} & \text{if } R_1 + \Delta \leq r_1 < R_2 \\ m & \text{if } R_2 \leq r_1 \end{cases} \end{aligned} \quad (2.12b)$$

The fugacity in the border regions is  $m_2 = m \exp(-U)$  where  $U < 0$  is the value of the external potential  $V(r)$  near the boundary. Notice that  $m_2 > m$ . It is clear that model I is the limit of model II when  $U \rightarrow 0$  and  $m_2 \rightarrow 1$  with the product  $m_2 = m$  finite.

For this model II, the following symmetrization of the problem explained below will be useful. If an external potential is acting differently on positive and negative particles, as in our case, to symmetrize the problem for the two types of particles, Comu and Jancovici [9] propose to define  $m_s(r)$  and  $V_s(r)$  by the relations

$$m_s(r) = m_-(r) \exp[-2sV(r)]; \quad s = 1 \quad (2.13)$$

where  $V_s(r)$  in general is different from the external  $V(r)$  potentials. Knowing that  $V_s(r)$  is constant in each region, in terms of the modified Green functions

$$g_{s_1 s_2}(r_1; r_2) = e^{s_1 V(r_1)} G_{s_1 s_2}(r_1; r_2) e^{s_2 V(r_2)} \quad (2.14)$$

the system of equations (2.9) can be shown to be equivalent to

$$\frac{h}{(m_-(r_1))^2} \frac{i}{\theta_{r_1}} g_-(r_1; r_2) = m_-(r_1) (r_1 - r_2) \quad (2.15)$$

$$\frac{e^{i\theta_{r_1}}}{m_-(r_1)} \theta_{r_1} \frac{i}{r_1} \theta_{r_1} g_-(r_1; r_2) = g_-(r_1; r_2) \quad (2.16)$$

where  $\theta$  is the Laplacian operator and

$$\begin{aligned} m_-(r) &= \begin{cases} m_0 = (m_+ m_2)^{1/2} & \text{if } r \text{ in regions 1 or 3;} \\ m & \text{if } r \text{ in region 2;} \end{cases} \end{aligned} \quad (2.17)$$

and the potential defined in Eq. (2.13) is given by

$$\exp(V(r)) = \begin{cases} (m_2 - m_1)^{1/4} & \text{if } r \text{ in regions 1 or 3;} \\ 1 & \text{if } r \text{ in region 2;} \end{cases} \quad (2.18)$$

In the two following sections we will apply the method presented here to obtain the grand potential and the density profiles of the system.

### III. THE PRESSURE

#### A. The grand potential

To find the pressure of the confined Coulomb system we proceed first to compute the grand potential. As shown in section II the grand potential is given by

$$= \ln \sum_i (1 + \lambda_i) \quad (3.1)$$

where  $\lambda_i$  are the eigenvalues of the operator  $K$  given by equation (2.2). The eigenvalue problem for  $K$  with eigenvalue  $\lambda$  and eigenvector  $(\psi_i)$  reads

$$m_-(r)\psi_i(r) = 2\partial_z\psi_i(r) \quad (3.2a)$$

$$m_+(r)\psi_i(r) = 2\partial_z\psi_i(r) \quad (3.2b)$$

These two equations can be combined into

$$\psi_i(r) = \frac{m_+(r)m_-(r)}{2} \quad (3.3)$$

We now detail the computation of the grand potential for the case of a Coulomb system confined in a disk. The annulus geometry follows similar calculations.

We will only use model I for the attracting potential on the boundary for the calculation of the grand potential. Using model I the fugacities inside the disk read

$$m_+(r) = m; \quad m_-(r) = m + \delta(r - R); \quad (3.4)$$

and outside the disk they vanish. Replacing these fugacities into the eigenvalue problem equations (3.2) we find that  $\psi_i(r)$  is a continuous function while  $\psi_i(r)$  is discontinuous at  $r = R$  due to the Dirac delta distribution in  $m_-(r)$ . The discontinuity of  $\psi_i(r)$  is given by

$$(\mathcal{R}^+; \lambda) - (\mathcal{R}; \lambda) = -(\mathcal{R}; \lambda) e^{\lambda} \quad (3.5)$$

Defining  $k = m = 1$ , inside the disk  $r < R$ ,  $\psi_i(r)$  obeys the equation

$$\psi_i(r) = k^2 \psi_i(r) \quad (3.6)$$

with solutions of the form

$$\psi_i(r; \lambda) = A_1 e^{i\lambda} I_{l-1}(kr) \quad (3.7)$$

and

$$\psi_i(r; \lambda) = A_1 e^{i(l-1)} I_{l-1}(kr) \quad (3.8)$$

where  $I_{l-1}$  is a modified Bessel function of order  $l$ . Outside the disk  $m_+ = m_+ = 0$  and the corresponding solutions to equations (3.2) are

$$\psi_i(r) = B_1 e^{i\lambda} r^l \quad (3.9)$$

$$\psi_i(r) = B_1 e^{i(l-1)} r^{l-1}; \quad (3.10)$$

In order to have vanishing solutions at  $r = 1$  it is necessary that

$$(\mathcal{R}^+; \lambda) = 0; \quad \text{if } l = 1 \quad (3.11a)$$

$$(\mathcal{R}; \lambda) = 0; \quad \text{if } l = 0 \quad (3.11b)$$

Using these boundary conditions together with the continuity of  $\psi_i$  at  $R$  and the discontinuity (3.5) of  $\psi_i$  at  $R$  gives the eigenvalue equation

$$I_{l-1} \frac{m R}{r} = 0 \quad \text{if } l = 0 \quad (3.12a)$$

$$I_l \frac{m R}{r} + I_{l-1} \frac{m R}{r} = 0 \quad \text{if } l = 1 \quad (3.12b)$$

The product appearing in equation (3.1) can be partially computed by recognizing that the lhs of the eigenvalue equation (3.12) for arbitrary  $l$  can be written as a Weierstrass product [3, 12, 14, 16]. Let us introduce the analytic functions

$$f_1^{(-)}(z) = I_l(mzR) l! \frac{2}{mzR} \quad (3.13)$$

$$f_1^{(+)}(z) = [I_l(mzR) + I_{l-1}(mzR)](l-1)! \frac{2}{mzR} \quad (3.14)$$

By construction the zeros of  $f_1^{(+)}$  are the inverse of the eigenvalues for  $l > 0$  and the zeros of  $f_1^{(-)}$  are the inverse eigenvalues for  $l = 0$ . Furthermore, since  $f_1^{(-)}(0) = 1$ ,  $f_1^{(0)}(0) = 0$  and  $f_1^{(+)}(z)$  is an even function it can be factorized as the Weierstrass product

$$f_1^{(-)}(z) = \prod_{l=1}^{\infty} \frac{1 - \frac{z}{l}}{1 - \frac{z}{l-1}} \quad (3.15)$$

where the product runs over all  $l$  solutions of equation (3.12) for a given  $l$ . Then we can conclude that the grand potential (3.1) is given by

$$= \sum_{l=0}^{\infty} \ln f_1^{(-)}(l) + \sum_{l=1}^{\infty} \ln f_1^{(+)}(l) \quad (3.16)$$

After shifting by one the index in the second sum and rearranging the expression we find the final result for the grand potential

$$\text{disk} = \text{hd} + \text{atd} \quad (3.17)$$

with

$$h_d = \sum_{l=0}^{\infty} \ln 1! \frac{2^l}{m R} I_l(m R) \quad (3.18)$$

which is the grand potential for a two-component plasma in a disk with hard wall boundaries [11] ( $\epsilon = 0$ ) and

$$a_{td} = \sum_{l=0}^{\infty} \ln 1 + \frac{I_{l+1}(m R)}{I_l(m R)} \quad (3.19)$$

is the contribution due to the attractive potential near the walls.

Now we turn our attention to the case of the Coulomb system confined in an annulus of inner radius  $R_1$  and outer radius  $R_2$ . In this case the position dependent

fugacity for the negative particles inside the annulus is given by

$$m(r) = m + {}_1(r - R_1) + {}_2(r - R_2) \quad (3.20)$$

The calculation of the grand potential follows the similar steps as above. One should solve the Laplacian eigenvalue problem with the appropriate boundary conditions given by the continuity of and the discontinuity of at  $R_1$  and  $R_2$ . After some straightforward calculations the final result for the grand potential is

$$h_{\text{annulus}} = h_a + a_{ta} \quad (3.21)$$

with

$$h_a = \sum_{l=0}^{\infty} \ln \frac{m R_1^{l+1}}{R_2^l} (I_l(m R_2) K_{l+1}(m R_1) + I_{l+1}(m R_1) K_l(m R_2)) \quad (3.22)$$

and

$$a_{ta} = \sum_{l=0}^{\infty} \ln 1 + \frac{I_l(m R_2) K_{l+1}(m R_1) - K_{l+1}(m R_2) I_l(m R_1)}{I_l(m R_2) K_{l+1}(m R_1) + I_{l+1}(m R_1) K_l(m R_2)} \\ \sum_{l=0}^{\infty} \ln 1 + \frac{I_{l+1}(m R_2) K_{l+1}(m R_1) - K_{l+1}(m R_2) I_{l+1}(m R_1)}{I_l(m R_2) K_{l+1}(m R_1) + I_{l+1}(m R_1) K_l(m R_2)} \quad (3.23)$$

The first term  $h_a$  is the grand potential for a two-dimensional two-component plasma confined in an annulus [11] with hard wall boundaries<sup>1</sup> ( $\epsilon = 0$ ) and the second term  $a_{ta}$  is the contribution to the grand potential due to the attractive nature of the walls.

It should be noted that all the sums (3.18), (3.19), (3.22) and (3.23) above are divergent and should be cut-off to obtain finite results. This is due to the fact that the two-component plasma of point particles is not stable against the collapse of particles of opposite sign for  $q^2 < 2$ . The cut-off  $N$  for the sums should be chosen of order  $R/a$  where  $R$  is the characteristic size of the system (for instance the radius of the disk in the disk case) and  $a$  can be interpreted as the hard-core diameter of the particles [9, 11].

## B. Finite-size corrections

It is instructive to study the behavior of the grand potential when the system is large. It has been known for some time that two-dimensional Coulomb systems in their conducting phase have a similar behavior to critical systems [11, 12]. In particular the grand potential of a two-dimensional Coulomb system confined in a domain of characteristic size  $L$  has a large- $L$  expansion

$$= AL^2 + BL + \frac{1}{6} \ln L + O(1) \quad (3.24)$$

similar to the one predicted by Cardy [17, 18] for critical systems. The first two terms are respectively the bulk grand potential and the surface contribution to the grand potential (the surface tension) and are non-universal. The logarithmic term is a universal finite-size correction to the grand potential, it does not depend on the microscopic detail of the system, only on the topology of the manifold where the system lives through the Euler number  $\chi$ . For a disk  $\chi = 1$  and for an annulus  $\chi = 0$ .

It is interesting to verify if this finite-size expansion holds for the systems studied here, in particular if the finite-size correction is modified by the special attractive

<sup>1</sup> Eq. (4.16) of Ref. [11] is incorrect, however the equation above (4.16) is correct and gives our result (3.22) for the grand potential

nature of the walls considered here.

Let us first consider the case of the disk geometry. We choose to auto the sum s (3.18) and (3.19) to a maximum value for  $l$  equal to  $R=a$  and the results given here are for  $a \neq 0$ . The finite-size expansion for large- $R$  of the hard wall contribution to the grand potential has already been computed in Ref. [11] with the result

$$\text{hd} = p_b R^2 + \text{hw} + \frac{1}{6} \ln(mR) + O(1) \quad (3.25)$$

where the bulk pressure  $p_b$  is given by

$$p_b = \frac{m^2}{2} \left( 1 + \ln \frac{2}{m} \right) \quad (3.26)$$

and the surface tension  $\text{hw}$  for hard walls is given by

$$\text{hw} = m \left( \frac{1}{4} - \frac{1}{2} \right) \quad (3.27)$$

We only need to compute the large- $R$  expansion of (3.19). This can be done expressing the Bessel function  $I_{l+1}(mR)$  as  $I_{l+1}(mR) = I_l^0(mR) + II_l(mR) = (mR)$ , using the Debye expansions [19] of the Bessel functions valid for large argument and large index

$$I_l(z) = \frac{e}{2(l^2 + z^2)^{1/4}} \left( 1 + \frac{3t}{241} + \frac{5t^3}{241} \right) \quad (3.28a)$$

$$I_l^0(z) = \frac{(l^2 + z^2)^{1/4} e}{2z} \left( 1 + \frac{9t}{241} + \frac{7t^3}{241} \right) \quad (3.28b)$$

with  $z = \frac{p}{l^2 + z^2} + \ln \frac{z}{\sqrt{l^2 + z^2}}$  and  $t = \frac{p}{l^2 + z^2}$ , and using the Euler-Maclaurin formula to transform the summation into an integral

$$\begin{aligned} f(l) &= \int_0^{z_N} f(x) dx + \frac{1}{2} [f(N) + f(0)] \quad (3.29) \\ &+ \frac{1}{12} [f'(N) - f'(0)] + \end{aligned}$$

After some calculations we find that (3.19) contributes only to the surface tension giving for the grand potential the final result

$$\text{disk} = p_b R^2 + 2R + \frac{1}{6} \ln(mR) + O(1) \quad (3.30)$$

where the surface tension is now given by

$$= \frac{m}{4} \ln \frac{2}{ma} + 1 + + \frac{1}{2} \ln( + 1) \quad (3.31)$$

We recover as expected the surface tension obtained in Ref. [3] for the same system but confined in a slab.

The universal logarithmic finite-size correction  $(l=6) \ln(mR)$  is still present and it is not modified by the presence of the attractive boundaries.

For the annulus geometry we are interested in the limit  $R_1 \neq 1$  and  $R_2 \neq 1$  with  $R_2=R_1$  finite. We proceed as

above, using also this time the Debye expansion for the Bessel functions [19]

$$K_1(z) = \frac{e}{2(l^2 + z^2)^{1/4}} \left( 1 + \frac{3t}{241} + \frac{5t^3}{241} \right) \quad (3.32a)$$

$$K_1^0(z) = \frac{(l^2 + z^2)^{1/4} e}{2z} \left( 1 + \frac{9t}{241} + \frac{7t^3}{241} \right) \quad (3.32b)$$

Using (3.28) and (3.32) one can notice that inside the logarithm in (3.22) the term  $I_{l+1}(mR_1)K_1(mR_2)$  is exponentially small when compared to  $I_l(mR_2)K_{l+1}(mR_1)$  since  $R_2 \gg R_1 \neq 1$ . Also in the contribution from the attractive boundaries (3.23) the dominant terms are

$$\begin{aligned} \text{ata} & \sum_{l=0}^{N-1} \ln \left( 1 + \frac{K_1(mR_1)}{K_{l+1}(mR_1)} \right) \\ & \sum_{l=0}^{N-1} \ln \left( 1 + \frac{I_l(mR_2)}{I_{l+1}(mR_2)} \right) \quad (3.33) \end{aligned}$$

Then, after some calculations we arrive to the final result

$$\text{annulus} = p_b (R_2^2 - R_1^2) + 12R_1 + 2R_2 + O(1) \quad (3.34)$$

The surface tension for each boundary is given by

$$i = \frac{m}{4} \left( i \ln \frac{2N}{R_i} + 1 \right) + i + \frac{1}{i} \ln(i+1) \quad (3.35)$$

where  $i=1$  for the inner boundary and  $i=2$  for the outer boundary. The cut-off  $N$  should be chosen [11] as  $R=a$  where here  $R = R_2 x^{x^2/(1-x^2)}$  with  $x = R_1/R_2$  in order to insure extensivity and recover for the bulk pressure  $p_b$  the same expression (3.26) as before. This, however, will give a slightly different expression for the surface tension than the one in Eq. (3.31). This is more related to the arbitrariness in the choice of the cut-off that for any physical reason. For instance, if one chooses a different prescription for the cut-off  $N$  in the sums (3.33):  $R_1=a$  in the first sum and  $R_2=a$  in the second one would retrieve exactly the expression (3.31) for the surface tension. Anyway, notice that the (divergent) dominant term of the surface tension when the cut-off  $a$  vanishes is in all cases

$$\frac{m}{4} \ln \frac{2}{ma} \quad (3.36)$$

for a wall with adhesivity  $\gamma$ .

In equation (3.34) we do not find any logarithmic finite-size correction. There are some terms of the form  $\ln R_2=R_1$  which are order 1 because  $R_2=R_1$  is finite. This is in accordance to the expected formula (3.24) for an annulus where the Euler number is  $\gamma=0$ . Here again the special attractive nature of the walls does not modify the universal finite-size correction.

As a conclusion to this part we might say that the logarithmic correction is really universal, not only it does not depend on the microscopic constitution of the system but also it is insensitive to the nature of the walls.

### C. The disjoining pressure

Let us first detail the case of the disk geometry. The pressure  $p$  is given in terms of the grand potential by

$$p = \frac{1}{2} \frac{\partial}{R \partial R} \quad (3.37)$$

Using equation (3.17) together with equations (3.18) and (3.19) gives

$$p = p_{hd} + p_{atd} \quad (3.38)$$

$$p_{hd} = \frac{m}{R} \sum_{l=0}^{\infty} \frac{I_{l+1}(mR)}{I_l(mR)} \quad (3.39)$$

and  $p_{atd}$  is the contribution to the pressure due to the attractive potential near the walls and it is given by

$$p_{atd} = \frac{m}{2R^2} \sum_{l=0}^{\infty} \frac{mR}{I_l(mR)} \frac{I_l^2(mR)}{I_{l+1}(mR)} \frac{I_{l+1}^2(mR)}{I_l(mR)} \frac{(2l+1)I_{l+1}(mR)I_l(mR)}{[I_l(mR) + I_{l+1}(mR)]} \quad (3.40)$$

To study the stability of the system against an external applied pressure one should study the disjoining pressure  $p_d = p - p_b$  defined as the difference of the pressure of the system and the pressure of an infinite system (the bulk pressure). Let us first consider the case  $\epsilon = 0$ . A proper way to subtract the bulk pressure from expression (3.39) is by using the equation of state of the infinite system [9]

$$p_b = \frac{1}{2} n_b + \frac{m^2}{4} \quad (3.41)$$

where  $n_b$  is the bulk total density. A simple scaling argument shows that for  $q^2 < 2$  the equation of state of the two-dimensional two-component plasma is [20]

$$p_b = [1 - (q^2=4)]n_b \quad (3.42)$$

For  $q^2 = 2$ , the case considered here, the introduction of a cutoff  $a$  is needed in order to avoid divergences but this breaks the scale invariance of the two-dimensional logarithmic Coulomb potential giving rise to the anomalous term ( $m^2=4$ ) in the equation of state. Notice that when the cutoff  $a \neq 0$  both  $p_b$  and  $n_b$  diverge and we have  $p_d = n_b = 1/2$  in accordance to the general equation of state (3.42).

Formally, the bulk density can be written as (see next section for details)

$$\begin{aligned} n_b &= \frac{m^2}{2} \frac{X^1}{I_1(mR)K_1(mR)} \\ &= \frac{m^2}{2} I_0 K_0 + 2 \sum_{l=1}^{\infty} \frac{X^1}{I_l K_l} \end{aligned} \quad (3.43)$$

In the above expression and below the omitted argument of the Bessel functions is  $mR$  unless stated otherwise. On the other hand using the Wronskian  $I_l K_{l+1} + I_{l+1} K_l = (1-mR)$  the hard disk pressure (3.39) can be formally written as

$$p_{hd} = \frac{m^2}{2} \sum_{l=0}^{\infty} \frac{X^1}{I_l} \frac{I_{l+1}^2 K_1}{I_1} + \sum_{l=1}^{\infty} \frac{X^1}{I_l K_1} \quad (3.44)$$

Then the disjoining pressure for  $\epsilon = 0$  is

$$p_{hd,disj} = \frac{m^2}{2} \sum_{l=0}^{\infty} \frac{X^1}{I_l} \frac{I_{l+1}^2 K_1}{I_1} \frac{I_0 K_0}{2} + \frac{1}{4} \quad (3.45)$$

Although the pressure  $p_{hd}$  and the bulk pressure  $p_b$  are divergent when the cutoff  $a$  vanishes, the disjoining pressure  $p_{hd,disj}$  in the case  $\epsilon = 0$  is well defined for  $a \neq 0$  and the series (3.45) is convergent.

A plot of the disjoining pressure  $p_{hd,disj}$  for a hard wall disk as a function of the radius  $R$  is shown in Figure 1. Notice that  $p_{hd,disj}$  is an increasing function of  $R$  and it is always negative. This shows that in the absence of the attractive potential on the walls the system is always unstable for any radius  $R$ . This is a common feature of the disk geometry with the slab geometry studied in our previous work [3]. The system without any attractive potential on the boundary ( $\epsilon = 0$ ) is naturally unstable.

For  $\epsilon \neq 0$ , the disjoining pressure  $p_d$  is given by

$$p_d = p_{hd,disj} + p_{atd} \quad (3.46)$$

with  $p_{atd}$  given by equation (3.40). Before proceeding one should be aware of an important fact. Although the

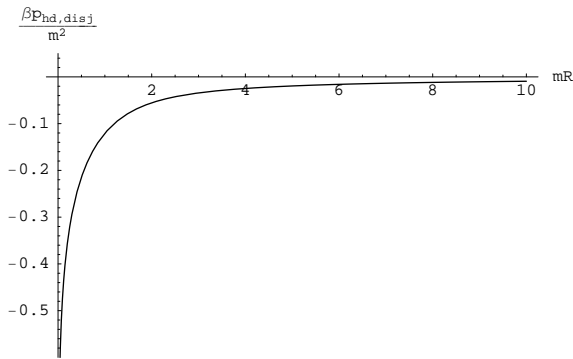


FIG. 1: The disjoining pressure  $p_{hd,disj}$  for the disk in the case of non-attractive boundaries ( $\gamma = 0$ ) as a function of the radius  $R$ . Notice that the disjoining pressure is always negative and it is an increasing function of the radius, indicating that the system is always unstable.

rst term  $p_{hd,disj}$  is nite when the cuto  $a \neq 0$  the second term on the other hand is divergent when  $a \neq 0$ . The sum in equation (3.40) should be cuto to a upper limit  $N = R/a$  as it was done in the preceding section. Rigorously speaking when  $a \neq 0$  the dominant term for the disjoining pressure is  $p_{atd}$ . For large radius  $R$ , from last section results (3.30) and (3.36) on the nite-size corrections we can deduce the dominant term of the disjoining pressure when  $a \neq 0$

$$p_d = \frac{1}{R} - \frac{m}{4R} \ln \frac{2}{ma} \quad (3.47)$$

This term is always positive and is a decreasing function of  $R$  indicating that the system is always stable.

This is an important difference between the slab geometry studied in Ref. [3] and the present case of the disk. In the slab geometry the disjoining pressure is always finite for  $a = 0$  and any value of  $\gamma$ . For a slab of width  $W$ , the large- $W$  expansion of the grand potential per unit area  $\Omega$  reads [3]

$$\Omega = p_b W + 2 + O(e^{-mW}) \quad (3.48)$$

Then the pressure  $p = \Omega/W$  does not contain any contribution from the surface tension. On the other hand in the disk geometry considered here the existence of the curvature makes the surface tension very relevant for the disjoining pressure (see equation (3.47)) and since diverges logarithmically with the cuto it plays a dominant role in the stability of the system.

Let us now consider a small but non-zero cuto  $a$ . It is expected that the results of our theory in that case should be close to the ones of a model of small hard-core particles of diameter  $a$ . Then there will be a competition between the natural unstable behavior of the case without attractive potential ( $\gamma = 0$ ) and the attractive part to the pressure  $p_{atd}$  which is stabilizing.

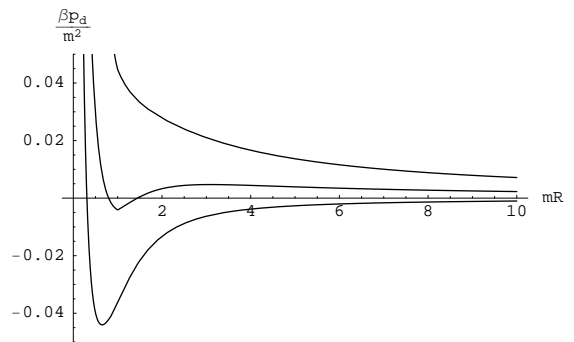


FIG. 2: The disjoining pressure  $p_d$  for the disk as a function of the radius  $R$  for  $\gamma = 0.15, 0.21$  and  $0.3$  from bottom to top. The cuto is chosen as  $ma = 10^3$ . The case  $\gamma = 0.3$  shows a stable disk for all radius, in the case  $\gamma = 0.15$  only small disks are stable and when  $\gamma = 0.21$  there is the possibility of a collapse from large disks to small disks.

Figure 2 shows several plots of the disjoining pressure  $p_d$  as a function of the radius  $R$  for three special values of the adhesivity  $\gamma = 0.15, 0.21$  and  $0.3$  for a fixed cuto  $ma = 10^3$ . These three plots show three characteristic regimes in which the system can be.

For large values of the adhesivity, for example the case  $\gamma = 0.3$  shown in the Figure 2, the disjoining pressure is always positive and a decreasing function of the radius  $R$ . This is a normal behavior: if the system is compressed the internal pressure increases. This indicates a stable system for all values of the radius  $R$ .

In the case  $\gamma = 0.15$  (small values of the adhesivity) we have two different behaviors of the disjoining pressure. For radius  $R$  smaller than a certain "critical" radius  $R_c$ , the disjoining pressure is a decreasing function of the radius  $R$ , indicating again a stable system. However, for radius  $R$  larger than  $R_c$  the disjoining pressure is an increasing function of the radius  $R$ . This behavior is anomalous, indicating that in this range of radius the system is not stable. A very large disk  $R \gg 1$  is marginally stable and will collapse to a disk of smaller radius  $R_a$  where  $R_a$  is the radius corresponding to  $p_d = 0$  (see Figure 3).

For  $\gamma = 0.21$  (intermediate values of the adhesivity) we have a crossover regime. There are now three different behaviors of the pressure characterized by two special radius  $R_c^{(1)}$  and  $R_c^{(2)}$ . For  $R < R_c^{(1)}$  the pressure is a decreasing function of  $R$ : a stable regime. Then for  $R_c^{(1)} < R < R_c^{(2)}$  the pressure is an increasing function of  $R$ : an unstable regime. Finally for  $R > R_c^{(2)}$  the pressure is again a decreasing function of  $R$ : another stable regime. One can do a Maxwell construction to determine the correct dependency of the pressure against the radius as shown in Figure 4. In this regime there is a first order transition (collapse) from a large (but finite) disk (radius  $R_b$ ) to smaller disk with radius  $R_a$  (see Figure 4).

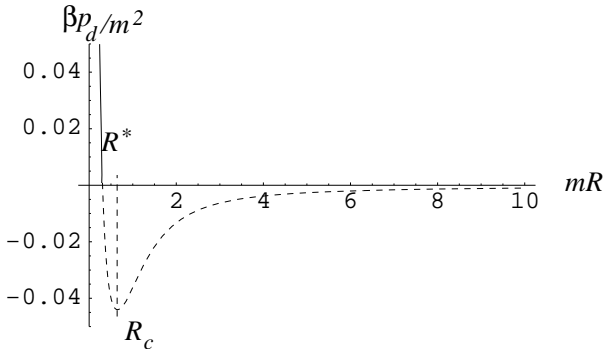


FIG. 3: The disjoining pressure  $p_d$  for the disk as a function of the radius  $R$  for  $\gamma = 0.15$ . The cutoff is chosen as  $a = 10^{-3}$ . The radius  $R_c$  is defined by  $\frac{\partial p_d}{\partial R} = 0$ . A very large disk  $R \gg 1$  would collapse to a disk of radius  $R_c$  with disjoining pressure  $p_d(R_c) = 0$ . The dashed region for  $R > R_c$  is not physical.

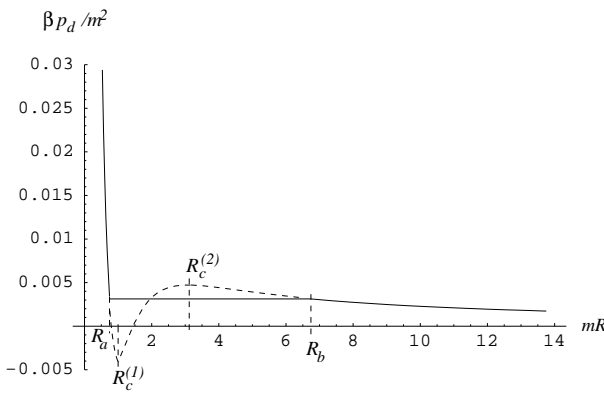


FIG. 4: The disjoining pressure  $p_d$  as a function of the radius  $R$  for  $\gamma = 0.21$  and a cutoff  $a = 10^{-3}$ . The theoretical result for the pressure shows a non-physical region (dashed line). The correct  $p_d$  vs.  $R$  curve can be obtained by a Maxwell construction, thus showing that in this case there is a first order transition (collapse) from a large disk (radius  $R_b$ ) to a small disk (radius  $R_a$ ).

Two of the three regimes illustrated here, small adhesivity (for example  $\gamma = 0.15$ ) and large adhesivity (for example  $\gamma = 0.3$ ), also occur for the slab geometry studied in Ref. [3]. In that case they were separated by the special value  $\gamma = \gamma_c = 1$ . The disk case considered here is however more rich since there is also a crossover regime between the two, for intermediate values of  $\gamma$  (for example  $\gamma = 0.21$ ), with the possibility of stable large radius  $R$  disks, a forbidden (unstable) intermediate range of radius  $R$  and then again stable small disks.

The values of  $\gamma$  characterizing the different regimes are however highly dependent on the cutoff and so are the values of the "critical" radius  $R_c$ ,  $R_c^{(1)}$  and  $R_c^{(2)}$ . The values  $\gamma = 0.15, 0.21$  and  $0.3$  of Figure 2 are for a cutoff  $a = 10^{-3}$ , for other values of the cutoff these values will change. For this reason the analysis above should be considered with some care. For very small values of the cutoff  $a$  we expect that the results obtained here should

reproduce asymptotically those of a primitive model of hard-core particles with radius  $a$ .

To conclude this section let us mention that in the annulus geometry the situation will be similar to the disk one. In that case one can consider the pressure on the inner boundary or the pressure on the outer boundary. For both pressures the dominant term when the cutoff  $a \ll 0$  will be given in terms of the surface tension as in equation (3.47). Then in the strict limit  $a \rightarrow 0$  the annulus geometry will be stable if  $\gamma > 0$  as in the disk case. Considering a small but non-zero cutoff  $a$  will lead to a similar discussion as in the disk with different regimes some of them exhibiting a collapse.

#### IV. THE DENSITY PROFILES

In this section, we study the densities of the Coulomb system confined inside a disk and inside an annulus. The densities can be obtained by computing the Green functions introduced in Sec. II. First we will solve and extensively study model I for the disk then the annulus. Then we will briefly consider the results that can be obtained using model II.

##### A. The disk

In the disk geometry, from model I, the fugacity  $m(r)$  is given by Eq. (2.10). From Eq. (2.9), when  $r_2 \notin R$ , we see that  $G_+$  and  $G_{++}$  are continuous for  $r_1 = R$ . However because of the Dirac delta distribution in the definition of  $m(r)$  the functions  $G_+$  and  $G_{++}$  are discontinuous at  $r_1 = R$ . The discontinuity can be obtained from Eq. (2.9) if  $r_2 \notin r_1$ :

$$G_+(r_1 = R; r_2) = G_+(r_1 = R^+; r_2) = e^{i\pi} G_+(r_1 = R; r_2) \quad (4.1)$$

If both points  $r_1$  and  $r_2$  are inside the disk but not on the boundary then Eq. (2.15) has solutions of the form

$$g_{s_1 s_2}(r_1; r_2) = \frac{m}{2} \sum_{l=1}^{X^1} e^{il(r_1 - r_2)} [I_1(m r_{<}) K_1(m r_{>}) + A_1(r_2) I_1(m r_1)] \quad (4.2)$$

where  $r_{<} = \min(r_1; r_2)$  and  $r_{>} = \max(r_1; r_2)$ . The remaining Green functions can be found using Eq. (2.16). In this model,  $e^{V(r)} = 1$  inside the system so  $g_{s_1 s_2}$  and  $G_{s_1 s_2}$  are the same.

If  $r_1$  is outside the disk while  $r_2$  is fixed inside the disk  $m_+(r_1) = m_-(r_1) = 0$ , the  $G_{s_1 s_2}$  that satisfy Eq. (2.9)

are

$$G_+ (r_1; r_2) = \frac{\mathbb{X}^1}{l=1} C_1(r_2; \pm) (r_1 e^{\pm i \frac{\pi}{4}})^l; \quad (4.3)$$

$$G_- (r_1; r_2) = \frac{\mathbb{X}^1}{l=1} D_1(r_2; \pm) (r_1 e^{\mp i \frac{\pi}{4}})^l; \quad (4.4)$$

So, in order to have finite solutions at  $r_1 = 1$  it is necessary that for  $r_1 > R$

$$\begin{aligned} C_1(r_2; \pm) &= 0 \quad \text{for } l \neq 0 \\ D_1(r_2; \pm) &= 0 \quad \text{for } l \neq 0; \end{aligned} \quad (4.5)$$

Eqs. (4.1) and (4.5) are the boundary conditions that complement the differential equations (2.15) and (2.16) for the Green functions.

Solving for the coefficients  $A_{\pm l}$ , we arrive at the following expressions for the Green functions for  $0 < r_{1,2} < R$ :

$$\begin{aligned} G_{++}(r_1; r_2) &= \frac{m}{2} K_0(m \mathbf{r}_1 - \mathbf{r}_2) \\ &+ \frac{m}{2} \sum_{l=1}^{\infty} \mathbb{X}^1 e^{il(\frac{\pi}{4} - \frac{\pi}{4})} A_{+l}^+ (m r_2) I_{l+1}(m r_1) \end{aligned} \quad (4.6)$$

where

$$A_{+l=0}^+(m r_2) = \frac{I_1(m r_2) K_{l+1}}{I_{l+1}} \quad (4.7)$$

$$A_{-l=0}^+(m r_2) = \frac{I_1(m r_2) (K_{l+1} - K_1)}{(I_{l+1} + I_1)} \quad (4.8)$$

and

$$\begin{aligned} G_{-}(r_1; r_2) &= \frac{m}{2} K_0(m \mathbf{r}_1 - \mathbf{r}_2) \\ &+ \frac{m}{2} \sum_{l=1}^{\infty} \mathbb{X}^1 e^{il(\frac{\pi}{4} - \frac{\pi}{4})} A_{-l}^- (m r_2) I_{l+1}(m r_1) \end{aligned} \quad (4.9)$$

where

$$A_{-l=0}^-(m r_2) = \frac{I_1(m r_2) K_1}{I_1} \quad (4.10)$$

$$A_{-l>0}^-(m r_2) = \frac{I_1(m r_2) (K_1 - K_{l+1})}{(I_1 + I_{l+1})} \quad (4.11)$$

with  $I_l$  meaning  $I_l(m R)$ , and the same convention for the Bessel function  $K_l$ .

From Eq. (2.16), one obtains

$$\begin{aligned} G_{-}(r_1; r_2) &= \frac{m}{2} \frac{r_1 e^{i \frac{\pi}{4}} - r_2 e^{i \frac{\pi}{4}}}{\mathbf{r}_1 - \mathbf{r}_2} K_1(m \mathbf{r}_1 - \mathbf{r}_2) \\ &+ \frac{m}{2} \sum_{l=1}^{\infty} \mathbb{X}^1 e^{il(\frac{\pi}{4} - \frac{\pi}{4})} i^{l+1} A_{-l}^- (m r_2) I_{l+1}(m r_1) \end{aligned} \quad (4.12)$$

The one-particle densities are given in terms of these Green functions as

$$s_1(r_1) = m s_1(r_1) G_{s_1 s_1}(r_1; r_1) \quad (4.13)$$

As we explained in section II the continuous limit model presents divergences in the expressions of the densities. This is seen in the term  $K_0(m r_{12})$  that diverges logarithmically as  $r_{12} = |\mathbf{r}_1 - \mathbf{r}_2| \rightarrow 0$ . So we impose a short distance cutoff. One can think that particles are disks of diameter  $a$ , so the minimal distance between particles is  $a$ .

Because of the form (2.10) of  $\rho(r)$ , the negative density can be written as

$$\rho(r) = 1 + \frac{m}{\pi} (r - R) \quad (4.14)$$

where  $\rho$  can be seen as the density of non-absorbed particles. For the positive particles  $\rho_+ = \rho_+$ . Finally we have

$$\rho(r) = \frac{m^2}{2} K_0(m a) + \sum_{l=1}^{\infty} \frac{\mathbb{X}^1}{l+1} A_{-l}^-(m r) I_{l+1}(m r) \quad (4.15)$$

The first term is the bulk density  $\rho_b$ , the density of the unbounded system as calculated in Ref. [9]. For  $a \ll R$

$$\rho_+ = \rho_b = \rho_b = \frac{m^2}{2} K_0(m a) - \frac{m^2}{2} \ln \frac{2}{m a} \quad (4.16)$$

where  $\gamma' = 0.5772$  is the Euler constant. In the second term of Eq. (4.15) the sum can eventually diverge for certain values of  $r$  (in the boundaries) so we should impose a cutoff  $|r| < N = R = a$  as it has been done in the expressions of the pressure and grand-potential obtained in the last section.

Rearranging the expression (4.15) for the densities one can obtain the results

$$+ (r) = b + \frac{m^2 X}{2} \sum_{l=0}^{\infty} \frac{K_l}{I_l} I_{l+1}^2 (m r) + \frac{K_{l+1}}{I_{l+1} + I_l} I_l^2 (m r) \quad (4.17a)$$

$$(r) = b - \frac{m^2 X}{2} \sum_{l=0}^{\infty} \frac{K_l}{I_l} I_{l+1}^2 (m r) + \frac{K_{l+1}}{I_{l+1} + I_l} I_{l+1}^2 (m r) \quad (4.17b)$$

The non-absorbed charge density  $=_+$  can be obtained from the above expression and using the Wronskian of the Bessel functions  $I_l K_{l+1} + I_{l+1} K_l = 1 = m R$ ,

$$(r) = \frac{m^2 X}{2 R} \sum_{l=0}^{\infty} \frac{I_{l+1}^2 (m r) + I_l^2 (m r)}{(I_{l+1} + I_l) I_l} \quad (4.18)$$

Finally, the total charge density

$$\begin{aligned} (r) &= + (r) - (r) \\ &= + (r) - 1 + \frac{m}{m} (r - R) - (r) \quad (4.19) \\ &= (r) - (r - R) \end{aligned}$$

has a non-absorbed part  $(r)$  and a absorbed \surface charge density in the boundary

$$= \frac{m}{m} (R) \quad (4.20)$$

This surface charge density comes from the  $(r - R)$  part of the negative charge density. Writing formally the bulk part of the density as  $b = (m^2/2) \sum_{l=0}^{\infty} I_l K_l$  one can obtain the following expression for  $b$  from Eqs. (4.20) and (4.17b)

$$= \frac{m^2 X}{2 R} \sum_{l=0}^{\infty} \frac{I_{l+1}}{I_{l+1} + I_l} \quad (4.21)$$

Actually the absorbed charge density should obey two special relations. The first is a sum rule that expresses the global electro-neutrality of the system

$$R = \int_0^R (r) r dr \quad (4.22)$$

Using the infinite integral

$$\int_0^R x (I_{l+1}^2 (x) + I_l^2 (x)) dx = \frac{(m R)^2}{2} I_{l+1}^2 - I_l I_{l+2} + I_l^2 - I_{l-1} I_{l+1} = m R I_l I_{l+1} \quad (4.23)$$

obtained using the recurrence relations [21] for the Bessel functions  $I_l$ , the sum rule (4.22) is immediately shown to be satisfied.

On the other hand the adhesivity  $\alpha$  can be thought as a sort of fugacity that controls the number of absorbed particles [1] and one can obtain the total number of absorbed particles  $2 R$  from the grand potential by using the usual thermodynamic relation

$$2 R = \frac{\partial \Omega_{\text{disk}}}{\partial \alpha} \quad (4.24)$$

This relationship is also immediately shown to be satisfied from the expression (3.19) for  $\Omega_{\text{atd}}$ , the part of the grand potential that depends on  $\alpha$ .

For a large disk,  $R \gg 1$ , the dominant part of the grand potential that depends on  $\alpha$  is the surface tension given by equations (3.31) and (3.36). Then we have

$$= \frac{\alpha}{\alpha} \quad (4.25)$$

a relation already shown to be true in Ref. [3] for the same system near a plane attractive hard wall. Using Eq. (3.31) into Eq. (4.25) gives explicitly

$$= \frac{m}{4} \ln \frac{2}{m a} \frac{\alpha^2 + 1}{\alpha^2 + 1} \ln(\alpha + 1) + 1 \quad (4.26)$$

Thus recovering a known result from Ref. [3]. Notice that for large disks the absorbed surface charge density becomes independent of the radius  $R$ .

In Figure 5, we can see the charge density profile  $(r)$  (actually only the non-absorbed part  $(r)$  is shown). It can be seen that the negative surface charge (not shown in the figure) is screened by a positive layer near  $r = R$ . As the adhesivity is increased,  $\alpha$  increases, and therefore the density of the screening positive layer shown in Figure 5 increases. This screening layer has a thickness of order of magnitude  $m^{-1}$  as expected since  $m^{-1}$  is a measure of the screening length [9].

In Figure 6, we can see the distribution of the negative particles (two lower curves) and positive particles (two

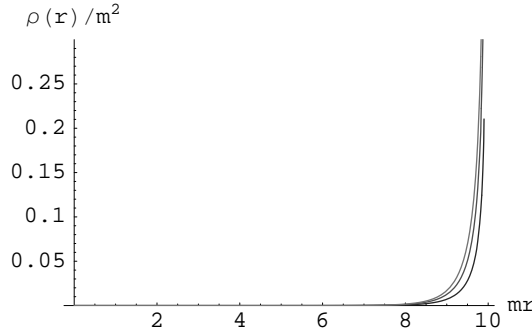


FIG. 5: The charge density profile  $\rho(r)$  for a disk of radius  $R = 10\text{m}$ . From bottom to top the adhesivity = 0.25; 0.5, 0.75.

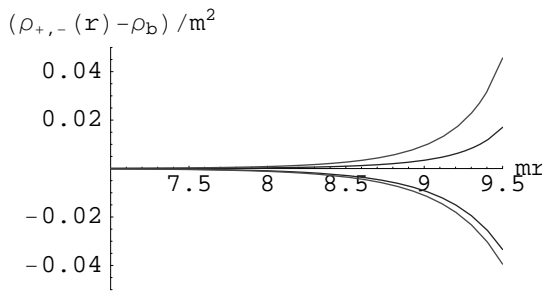


FIG. 6: The density profiles  $\rho_+(r)$  and  $\rho_-(r)$  for a disk of radius  $R = 10\text{m}$ . The bulk density has been subtracted from both densities. The upper curves correspond to the density of the positive particles  $\rho_+(r)$  and the bottom curves to the density of the negative particles  $\rho_-(r)$ . The adhesivity = 1 for the topmost curve ( $\rho_+(r)$ ) and the bottommost curve ( $\rho_-(r)$ ). The two other curves correspond to  $\alpha = 0.5$ .

upper curves). The negative particles feel repelled by the ones that lie in the boundary (the surface charge  $\rho_0$ ). Therefore, the negative density  $\rho_-(r)$  decreases near the frontier. The positive charge density  $\rho_+(r)$  inside the disk can be observed in the upper curves of Figure 6. Due to the large accumulation of negative charges at the frontier, the positive particles tend to shield this charge. Hence, there is an increase of the positive density near  $R$ .

As we increase the adhesivity, the negative absorbed charge on the border gets larger while on the inner region there is a stronger repulsion of the negative charges and an increase in the number of positive particles shielding the outer charge.

### B. The Annulus

For the annulus geometry with a delta distribution modeling the external attractive potential (model I), we follow the same reasonings as for the disk geometry. The solution to Eq. (2.15) for  $R_1 < r < R_2$  is of the form

$$G_{+-}(r_1; r_2) = \frac{m}{2} \sum_{l=1}^{X^1} e^{il_{12}} [I_1(m r_1) K_1(m r_2) + A_1(r_2) I_1(m r_1) + B_1(r_2) K_1(m r_1)] \quad (4.27)$$

where we defined  $l_{12} = l_1 - l_2$ . As in the disk case, the Green functions  $G_{-+}$  and  $G_{+-}$  are continuous while  $G_{++}$  and  $G_{--}$  are discontinuous at  $r = R_1$  and  $r = R_2$  with a discontinuity given by Eq. (4.1) replacing the adhesivity by  $\alpha_1$  for the discontinuity at  $r = R_1$  and by  $\alpha_2$  for the discontinuity at  $r = R_2$ .

Solving for the coefficients we finally find

$$G_{+-}(r_1; r_2) = \frac{m}{2} \left[ K_0(m |r_1 - r_2|) + \sum_{l=1}^{X^1} e^{il_{12}} [A_1(r_2) I_1(m r_1) + B_1(r_2) K_1(m r_1)] \right] \quad (4.28)$$

with

$$A_{1-0}(r_2) = \frac{I_1(m r_2)K_1^{(2)} - K_1^{(1)} + K_1^{(1)}}{I_1^{(2)} - I_1^{(1)} + K_1^{(1)}} \quad (4.29a)$$

$$B_{1-0}(r_2) = \frac{K_1(m r_2)I_1^{(2)} - I_1(m r_2)K_1^{(2)} - I_1^{(1)}}{I_1^{(2)} - I_1^{(1)} + K_1^{(1)}} \quad (4.29b)$$

$$A_{1>0}(r_2) = \frac{K_1(m r_2)I_1^{(1)} - I_1(m r_2)K_1^{(1)} - 2K_1^{(2)} + K_1^{(2)}}{I_1^{(1)} - 2K_1^{(2)} - K_1^{(2)} + K_1^{(1)} - 2I_1^{(2)} + I_1^{(2)}} \quad (4.29c)$$

$$B_{1>0}(r_2) = \frac{I_1(m r_2)I_1^{(1)} - 2K_1^{(2)} - K_1^{(2)} + K_1(m r_2)I_1^{(1)} - 2I_1^{(2)} + I_1^{(2)}}{I_1^{(1)} - 2K_1^{(2)} - K_1^{(2)} + K_1^{(1)} - 2I_1^{(2)} + I_1^{(2)}} \quad (4.29d)$$

and

$$G_{++}(r_1; r_2) = \frac{m}{2} \left[ K_0(m |r_1 - r_2|) + \sum_{l=1}^{\infty} e^{il r_2} [A_{1+}^+(r_2)I_1(m r_1) + B_{1+}^+(r_2)K_1(m r_1)] \right] \quad (4.30)$$

with

$$A_{1<0}^+(r_2) = \frac{I_1(m r_2)K_{1+1}^{(2)} - I_1^{(1)} + K_1^{(1)} + K_1(m r_2)K_{1+1}^{(2)} - I_1^{(1)} + I_1^{(1)}}{I_{1+1}^{(2)} - I_{1+1}^{(1)} + K_1^{(1)}} \quad (4.31a)$$

$$B_{1<0}^+(r_2) = \frac{K_1(m r_2)I_{1+1}^{(2)} + I_1(m r_2)K_{1+1}^{(2)} - I_{1+1}^{(1)} + I_1^{(1)}}{I_{1+1}^{(2)} - I_{1+1}^{(1)} + K_1^{(1)}} \quad (4.31b)$$

$$A_{1>0}^+(r_2) = \frac{K_1(m r_2)I_{1+1}^{(1)} + I_1(m r_2)K_{1+1}^{(1)} - 2K_{1+1}^{(2)} + K_1^{(2)}}{I_{1+1}^{(1)} - 2K_{1+1}^{(2)} - K_1^{(2)} + K_{1+1}^{(1)} - 2I_{1+1}^{(2)} + I_1^{(2)}} \quad (4.31c)$$

$$B_{1>0}^+(r_2) = \frac{I_1(m r_2)I_{1+1}^{(1)} - 2K_{1+1}^{(2)} - K_1^{(2)} + K_1(m r_2)I_{1+1}^{(1)} - 2I_{1+1}^{(2)} + I_1^{(2)}}{I_{1+1}^{(1)} - 2K_{1+1}^{(2)} - K_1^{(2)} + K_{1+1}^{(1)} - 2I_{1+1}^{(2)} + I_1^{(2)}} \quad (4.31d)$$

where  $I_1^{(1)} = I_1(m R_1)$ ,  $I_1^{(2)} = I_1(m R_2)$  and the same convention for the other Bessel functions.

These expressions can eventually be arranged to show explicitly the symmetry between  $r_1$  and  $r_2$ ,

$$G(r_1, r_2) = \frac{m}{2} K_0 (m \hat{r}_1 \cdot \hat{r}_2) \quad (4.32a)$$

$$+ \frac{m}{2} \sum_{l=0}^{\infty} \frac{e^{i l \cdot \hat{r}_2} K_1^{(2)} \cdot K_1^{(1)} + K_{l+1}^{(1)}}{I_1^{(2)} \cdot K_1^{(1)} + K_{l+1}^{(1)} \cdot K_1^{(2)} \cdot I_1^{(1)} \cdot I_{l+1}^{(1)}} I_1(m r_1) I_1(m r_2) \quad (4.32b)$$

$$+ \frac{m}{2} \sum_{l=0}^{\infty} \frac{e^{i l \cdot \hat{r}_2} I_1^{(2)} \cdot I_1^{(1)} \cdot I_{l+1}^{(1)}}{I_1^{(2)} \cdot K_1^{(1)} + K_{l+1}^{(1)} \cdot K_1^{(2)} \cdot I_1^{(1)} \cdot I_{l+1}^{(1)}} K_1(m r_1) K_1(m r_2) \quad (4.32c)$$

$$+ \frac{m}{2} \sum_{l=0}^{\infty} \frac{e^{i l \cdot \hat{r}_2} K_1^{(2)} \cdot I_1^{(1)} \cdot I_{l+1}^{(1)} \cdot [I_1(m r_1) K_1(m r_2) + K_1(m r_1) I_1(m r_2)]}{I_1^{(2)} \cdot K_1^{(1)} + K_{l+1}^{(1)} \cdot K_1^{(2)} \cdot I_1^{(1)} \cdot I_{l+1}^{(1)}} \quad (4.32d)$$

$$+ \frac{m}{2} \sum_{l=0}^{\infty} \frac{e^{i(l+1) \cdot \hat{r}_2} K_{l+1}^{(1)} \cdot 2K_{l+1}^{(2)} \cdot K_1^{(2)}}{I_{l+1}^{(1)} \cdot 2K_{l+1}^{(2)} \cdot K_1^{(2)} \cdot K_{l+1}^{(1)} \cdot 2I_{l+1}^{(2)} + I_1^{(2)}} I_{l+1}(m r_1) I_{l+1}(m r_2) \quad (4.32e)$$

$$+ \frac{m}{2} \sum_{l=0}^{\infty} \frac{e^{i(l+1) \cdot \hat{r}_2} I_{l+1}^{(1)} \cdot 2I_{l+1}^{(2)} + I_1^{(2)}}{I_{l+1}^{(1)} \cdot 2K_{l+1}^{(2)} \cdot K_1^{(2)} \cdot K_{l+1}^{(1)} \cdot 2I_{l+1}^{(2)} + I_1^{(2)}} K_{l+1}(m r_1) K_{l+1}(m r_2) \quad (4.32f)$$

$$+ \frac{m}{2} \sum_{l=0}^{\infty} \frac{e^{i(l+1) \cdot \hat{r}_2} I_{l+1}^{(1)} \cdot 2K_{l+1}^{(2)} \cdot K_1^{(2)} \cdot h \cdot i \cdot [K_{l+1}(m r_1) I_{l+1}(m r_2) + I_{l+1}(m r_1) K_{l+1}(m r_2)]}{I_{l+1}^{(1)} \cdot 2K_{l+1}^{(2)} \cdot K_1^{(2)} \cdot K_{l+1}^{(1)} \cdot 2I_{l+1}^{(2)} + I_1^{(2)}} \quad (4.32g)$$

and

$$G_{++}(r_1, r_2) = \frac{m}{2} K_0 (m \hat{r}_1 \cdot \hat{r}_2) \quad (4.33a)$$

$$+ \frac{m}{2} \sum_{l=0}^{\infty} \frac{e^{i(l+1) \cdot \hat{r}_2} K_1^{(2)} \cdot h \cdot K_1^{(1)} + K_{l+1}^{(1)} \cdot i}{I_1^{(2)} \cdot K_1^{(1)} + K_{l+1}^{(1)} \cdot K_1^{(2)} \cdot I_1^{(1)} \cdot I_{l+1}^{(1)}} I_{l+1}(m r_1) I_{l+1}(m r_2) \quad (4.33b)$$

$$+ \frac{m}{2} \sum_{l=0}^{\infty} \frac{e^{i(l+1) \cdot \hat{r}_2} I_1^{(2)} \cdot h \cdot I_1^{(1)} \cdot I_{l+1}^{(1)}}{I_1^{(2)} \cdot K_1^{(1)} + K_{l+1}^{(1)} \cdot K_1^{(2)} \cdot I_1^{(1)} \cdot I_{l+1}^{(1)}} K_{l+1}(m r_1) K_{l+1}(m r_2) \quad (4.33c)$$

$$+ \frac{m}{2} \sum_{l=0}^{\infty} \frac{e^{i(l+1) \cdot \hat{r}_2} K_1^{(2)} \cdot I_1^{(1)} \cdot I_{l+1}^{(1)} \cdot [I_{l+1}(m r_1) K_{l+1}(m r_2) + K_{l+1}(m r_1) I_{l+1}(m r_2)]}{I_1^{(2)} \cdot K_1^{(1)} + K_{l+1}^{(1)} \cdot K_1^{(2)} \cdot I_1^{(1)} \cdot I_{l+1}^{(1)}} \quad (4.33d)$$

$$+ \frac{m}{2} \sum_{l=0}^{\infty} \frac{e^{i l \cdot \hat{r}_2} K_{l+1}^{(1)} \cdot 2K_{l+1}^{(2)} \cdot K_1^{(2)} \cdot h \cdot i}{I_{l+1}^{(1)} \cdot 2K_{l+1}^{(2)} \cdot K_1^{(2)} \cdot K_{l+1}^{(1)} \cdot 2I_{l+1}^{(2)} + I_1^{(2)}} I_1(m r_1) I_1(m r_2) \quad (4.33e)$$

$$+ \frac{m}{2} \sum_{l=0}^{\infty} \frac{e^{i l \cdot \hat{r}_2} I_{l+1}^{(1)} \cdot 2I_{l+1}^{(2)} + I_1^{(2)}}{I_{l+1}^{(1)} \cdot 2K_{l+1}^{(2)} \cdot K_1^{(2)} \cdot K_{l+1}^{(1)} \cdot 2I_{l+1}^{(2)} + I_1^{(2)}} K_1(m r_1) K_1(m r_2) \quad (4.33f)$$

$$+ \frac{m}{2} \sum_{l=0}^{\infty} \frac{e^{i l \cdot \hat{r}_2} I_{l+1}^{(1)} \cdot 2K_{l+1}^{(2)} \cdot K_1^{(2)} \cdot h \cdot i \cdot [I_1(m r_1) K_1(m r_2) + K_1(m r_1) I_1(m r_2)]}{I_{l+1}^{(1)} \cdot 2K_{l+1}^{(2)} \cdot K_1^{(2)} \cdot K_{l+1}^{(1)} \cdot 2I_{l+1}^{(2)} + I_1^{(2)}} \quad (4.33g)$$

The individual densities are obtained putting  $r_1 = r_2 = r$  in the above expressions since  $s(r) = m_s(r) G_{ss}(r; r)$ . The above expressions are quite long, however one can notice some symmetries between  $G$  and  $G_{++}$ . Beside a change of sign and the phase factor (which is irrelevant in the calculation of the densities) the coefficient of the term

$I_1(m r_1)I_1(m r_2)$  in  $G$  is the same as the one for  $I_{1+1}(m r_1)I_{1+1}(m r_2)$  in  $G_{++}$  and so on. The charge density can be written again as

$$(r) = (r) \quad (1) \quad (r - R_1) \quad (2) \quad (r - R_2) \quad (4.34)$$

with a non-absorbed part  $(r)$  and a surface density

$$(1;2) = (1;2) \quad (R_{1;2}) \quad (4.35)$$

of absorbed negative particles in  $R_1$  and  $R_2$  respectively. The non-absorbed charge density is

$$(r) = \frac{m^2 X}{2} \sum_{l=0}^{\infty} \left[ (C_{1;l}^{II} + C_{2;l}^{II}) I_{1+1}^2(m r) + I_1^2(m r) + (C_{1;l}^{KK} + C_{2;l}^{KK}) K_{1+1}^2(m r) + K_1^2(m r) \right. \\ \left. + 2(C_{1;l}^{IK} + C_{2;l}^{IK}) [I_{1+1}(m r)K_{1+1}(m r) - I_1(m r)K_1(m r)] \right] \quad (4.36)$$

with the coefficients that depend on  $l$  given by

$$C_{1;l}^{II} = \frac{K_1^{(2)} h_{1K_1^{(1)}} + K_{1+1}^{(1)} i_{1K_1^{(1)}}}{I_1^{(2)} h_{1K_1^{(1)}} + K_{1+1}^{(1)} K_1^{(2)} h_{1I_1^{(1)}} - I_{1+1}^{(1)}} \quad (4.37a)$$

$$C_{1;l}^{KK} = \frac{h_{1K_1^{(1)}}}{I_1^{(2)} h_{1K_1^{(1)}} + K_{1+1}^{(1)} K_1^{(2)} h_{1I_1^{(1)}} - I_{1+1}^{(1)}} \quad (4.37b)$$

$$C_{1;l}^{IK} = \frac{K_1^{(2)} h_{1I_1^{(1)}} + I_{1+1}^{(1)}}{I_1^{(2)} h_{1K_1^{(1)}} + K_{1+1}^{(1)} K_1^{(2)} h_{1I_1^{(1)}} - I_{1+1}^{(1)}} \quad (4.37c)$$

and the ones that depend on  $l$  are

$$C_{2;l}^{II} = \frac{K_{1+1}^{(1)} h_{2K_{1+1}^{(2)}} + K_1^{(2)} i_{2K_{1+1}^{(2)}}}{I_{1+1}^{(1)} h_{2K_{1+1}^{(2)}} + K_1^{(2)} K_{1+1}^{(1)} h_{2I_{1+1}^{(2)}} + I_1^{(2)}} \quad (4.38a)$$

$$C_{2;l}^{KK} = \frac{h_{2K_{1+1}^{(2)}}}{I_{1+1}^{(1)} h_{2K_{1+1}^{(2)}} + K_1^{(2)} K_{1+1}^{(1)} h_{2I_{1+1}^{(2)}} + I_1^{(2)}} \quad (4.38b)$$

$$C_{2;l}^{IK} = \frac{K_{1+1}^{(1)} h_{2K_{1+1}^{(2)}} + K_1^{(2)} i_{2K_{1+1}^{(2)}}}{I_{1+1}^{(1)} h_{2K_{1+1}^{(2)}} + K_1^{(2)} K_{1+1}^{(1)} h_{2I_{1+1}^{(2)}} + I_1^{(2)}} \quad (4.38c)$$

The absorbed charge density in each boundary can be computed by replacing  $G$  ( $R_{1;2}; R_{1;2}$ ) from Eq. (4.32) into Eq. (4.35) or by using the thermodynamic relation

$$2 R_{1;2} (1;2) = \frac{\mathcal{E}_{\text{annulus}}}{\mathcal{E}_{1;2}} \quad (4.39)$$

Either way the result is the same as expected

$$(1) = \frac{1}{2 R_1} \sum_{l=0}^{\infty} \frac{I_1^{(2)} K_1^{(1)} + K_{1+1}^{(2)} I_1^{(1)}}{I_1^{(2)} h_{1K_1^{(1)}} + K_{1+1}^{(1)} K_1^{(2)} h_{1I_1^{(1)}} - I_{1+1}^{(1)}} \quad (4.40a)$$

$$(2) = \frac{2}{2 R_2} \sum_{l=0}^{\infty} \frac{I_{1+1}^{(2)} K_{1+1}^{(1)} + K_{1+1}^{(2)} I_1^{(1)}}{I_{1+1}^{(1)} h_{2K_{1+1}^{(2)}} + K_1^{(2)} K_{1+1}^{(1)} h_{2I_{1+1}^{(2)}} + I_1^{(2)}} \quad (4.40b)$$

Using the infinite integrals (4.23) and [22]

$$\int_{mR}^{\infty} (K_{1+1}^2(x) + K_{1+1}^2(x)) x dx = mR K_{1+1} K_1 \quad (4.41)$$

$$\int_{mR}^{\infty} (I_{1+1}(x) K_{1+1}(x) - I_1(x) K_1(x)) x dx = \frac{mR}{2} (K_{1+1} I_1 - I_{1+1} K_1) \quad (4.42)$$

one can verify that the electroneutrality sum rule

$$\int_{R_1}^{R_2} (r) r dr = R_1^{(1)} + R_2^{(2)} \quad (4.43)$$

is satisfied. Indeed after performing the integrals and doing some manipulations using the Wronskian relations we find for the part that depends on  $r_1$

$$\begin{aligned} & \int_{mR_1}^{mR_2} C_{1,1}^{II} I_{1+1}^2(x) + I_1^2(x) + C_{1,1}^{KK} K_{1+1}^2(x) + K_1^2(x) + 2C_{1,1}^{IK} [I_{1+1}(x) K_{1+1}(x) - I_1(x) K_1(x)] x dx = \\ & = 1 \frac{K_1^{(1)} I_1^{(2)} - K_1^{(2)} I_1^{(1)}}{I_1^{(2)} - I_1^{(1)} K_1^{(1)} + K_{1+1}^{(1)}} + mR_2 K_1^{(2)} I_{1+1}^{(2)} - mR_1 I_{1+1}^{(1)} K_1^{(1)} \end{aligned} \quad (4.44)$$

while for the part that depends on  $r_2$

$$\begin{aligned} & \int_{mR_1}^{mR_2} C_{2,1}^{II} I_{1+1}^2(x) + I_1^2(x) + C_{2,1}^{KK} K_{1+1}^2(x) + K_1^2(x) + 2C_{2,1}^{IK} [I_{1+1}(x) K_{1+1}(x) - I_1(x) K_1(x)] x dx = \\ & = 2 \frac{I_{1+1}^{(1)} K_{1+1}^{(2)} - K_{1+1}^{(1)} I_{1+1}^{(2)}}{I_{1+1}^{(1)} - I_{1+1}^{(2)} K_1^{(2)} - K_1^{(2)}} + mR_2 K_1^{(2)} I_{1+1}^{(2)} + mR_1 I_{1+1}^{(1)} K_1^{(1)} \end{aligned} \quad (4.45)$$

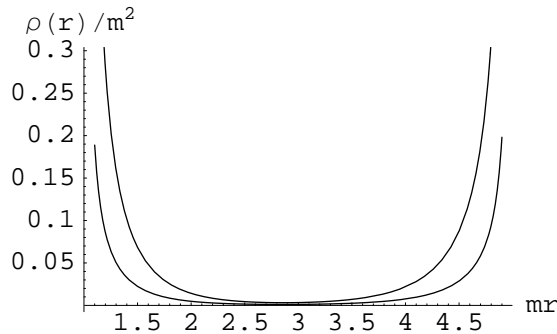


FIG. 7: The charge density profile  $\rho(r)$  for an disk of inner radius  $R_1 = 1m$  and outer radius  $R_2 = 5m$ . The adhesivities in each boundary have been chosen equals  $\alpha_1 = \alpha_2 = \alpha$ . The upper curve correspond to  $\alpha = 1$  while the lower one to  $\alpha = 0.25$ .

Adding both results from Eqs. (4.44) and (4.45) the terms independent from  $r_1$  and  $r_2$  cancel out while the rest is the contribution for  $r_1^{(1)}$  and  $r_2^{(2)}$  respectively, thus recovering the electro-neutrality sum rule Eq. (4.43).

Figure 7 shows a plot of the charge density  $\rho(r)$  for an annulus with inner radius  $R_1 = 1m$  and outer radius

$R_2 = 5m$  for  $\alpha_1 = \alpha_2 = 0.5$  and  $\alpha_1 = \alpha_2 = 1$ . In both figures one can see a positive layer of charge in each boundary screening the absorbed negative surface charge densities  $r_1^{(1,2)}$ . As  $r_1^{(1,2)}$  increases the absorbed charge increases and so does the positive layer. Although it is not perfectly clear in Figure 7 there is actually slightly more absorbed surface charge density in the inner boundary than in the outer. This can be seen in Figure 8 that shows the difference between the absorbed surface charge in the inner boundary and the surface charge in the outer one:  $r_1^{(1)} - r_2^{(2)}$ . Figure 8 clearly shows that  $r_1^{(1)} > r_2^{(2)}$  if  $\alpha_1 = \alpha_2$ . On the other hand the total charge on the inner boundary is smaller than the total charge on the outer boundary:  $2R_1 r_1^{(1)} < 2R_2 r_2^{(2)}$ . This can be seen directly from Eqs. (4.40). If  $\alpha_1 = \alpha_2 = \alpha$ , each term in the series of the difference  $R_1 r_1^{(1)} - R_2 r_2^{(2)}$  from Eqs. (4.40) is of the form

$$\frac{b_1}{D_1^{(1)} D_1^{(2)}} (b_1 - b_{1+1}) \quad (4.46)$$

where  $D_1^{(1)}$  and  $D_1^{(2)}$  are the denominators in each term of the sum in Eqs. (4.40a) and (4.40b) respectively, and  $b_1 = K_1^{(1)} I_1^{(2)} - K_1^{(2)} I_1^{(1)}$ . The sequence  $(b_1)_{12N}$  has the property of being monotonically increasing with  $l$ . Then

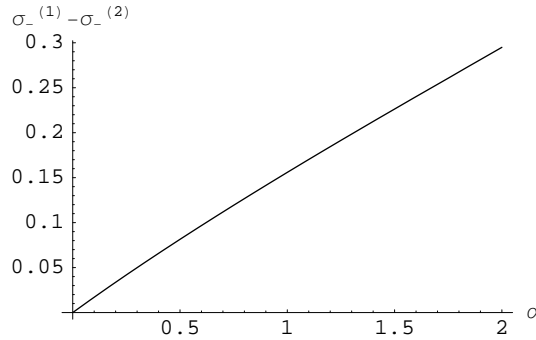


FIG. 8: The difference between the surface charge in the inner boundary and the surface charge in the outer one  $\sigma_{-}^{(1)} - \sigma_{-}^{(2)}$  as a function of  $\alpha$  for an annulus of inner radius  $R_1 = 1=m$  and outer radius  $R_2 = 5=m$ .

we conclude  $R_1^{(1)} < R_2^{(2)}$ .

### C. Model II

We now briefly consider model II and some of its results in the annulus geometry. Let us recall that in this model the fugacity of the negative particles is a step function given by Eq. (2.12). To obtain the Green functions  $g_{ss}$  we solve Eq. (2.15) which is a standard inhomogeneous Helmholtz equation in each region: inner border  $R_1 < r < R_1 + \delta$  (region 1), bulk  $R_1 + \delta < r < R_2$  (region 2) and outer border  $R_2 < r < R$  (region 3). Outside the annulus  $r < R_1$  and  $r > R_2$  the fugacities vanish and the equation satisfied by  $G_{ss}$  is the Laplace equation. The Green functions  $G_{s_1 s_2}$  are continuous at each boundary  $r = R_1$ ,  $r = R_1 + \delta$ ,  $r = R_2$  and  $r = R_2 - \delta$ . Remember that here the Green functions  $G_{s_1 s_2}$  are different from the auxiliary functions  $g_{s_1 s_2}$ . Their relationship is given by Eq. (2.14). While the Green functions  $G_{s_1 s_2}$  are continuous, the auxiliary Green functions  $g_{s_1 s_2}$  are in general discontinuous at the interfaces.

In the regions of interest, the form of the solution is, in general,

$$g_{ss}(r_1; r_2) = \frac{m(r_1)}{2} e^{i\ell(r_1 - r_2)} [I_1(m(r_1)r_1)K_1(m(r_1)r_1) + B_1(r_2)I_1(m(r_1)r_1) + C_1(r_2)K_1(m(r_1)r_1)] \quad (4.47)$$

with  $m(r) = m_0$  in the border regions 1 and 3 and  $m(r) = m$  in the bulk region 2. Imposing the continuity of the Green functions  $G_{s_1 s_2}$  gives a linear system of six equations for the coefficients  $B_1$  and  $C_1$  (there are six coefficients, two per region). Actually for each Green function  $G_{ss}$  one has to solve two linear systems of equations depending on the sign of  $\ell$ , thus in total one should solve four linear systems to obtain all coefficients. This

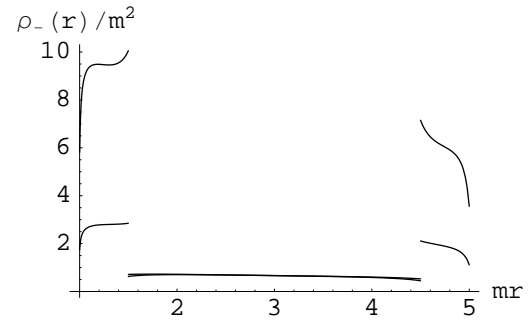


FIG. 9: The density profile of the negative particles for an annulus with inner radius  $R_1 = 1=m$ , outer radius  $R_2 = 5=m$  in model II. The width of the borders are  $\delta = 0.5=m$ . The fugacity in the border regions is: for the upper curve  $m_2 = 16m$  corresponding to a value of  $m_0 = 4m$  and for the lower curve  $m_2 = 4m$  corresponding to a value of  $m_0 = 2m$ . The cut-off in the sums of Bessel functions in the expression of the density has been chosen as  $N = 100$ .

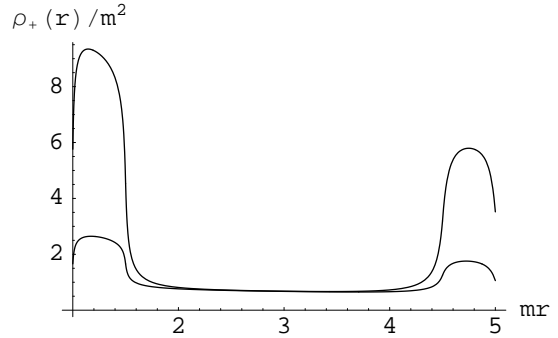


FIG. 10: The density profile of the positive particles for an annulus with inner radius  $R_1 = 1=m$ , outer radius  $R_2 = 5=m$  in model II. The width of the borders are  $\delta = 0.5=m$ . The fugacity in the border regions is: for the upper curve  $m_2 = 16m$  corresponding to a value of  $m_0 = 4m$  and for the lower curve  $m_2 = 4m$  corresponding to a value of  $m_0 = 2m$ . The cut-off in the sums of Bessel functions in the expression of the density has been chosen as  $N = 100$ .

can be conveniently done with the aid of matrix algebra software like Mathematica.

The explicit expression of the coefficients obtained from the solution of the linear systems [15] are too long to reproduce here, however we show in Figures 9, 10 and 11 some plots of the negative, positive, and charge density profiles for two values of  $m_2$ ,  $m_2 = 16m$  and  $m_2 = 4m$ .

Figure 9 shows the density profile of the negative particles. As expected there is a higher density of particles in the borders than in the bulk: for higher values of the fugacity  $m_2$  in the border (the external potential  $V(r)$  is more attractive), the density in the borders is higher. Also the density profile is discontinuous at the interfaces. This is expected for the negative particles since the potential  $V(r)$  is discontinuous across the interfaces.

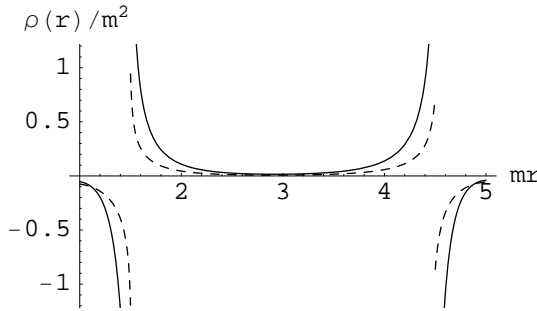


FIG. 11: The charge density profile for an annulus with inner radius  $R_1 = 1=m$ , outer radius  $R_2 = 5=m$  in model II. The width of the borders are  $\delta = 0.5=m$ . The fugacity in the border regions is: for the solid line curve  $m_2 = 16m$  corresponding to a value of  $m_0 = 4m$  and for the dashed line curve  $m_2 = 4m$  corresponding to a value of  $m_0 = 2m$ . The cutoff in the sums of Bessel functions in the expression of the density has been chosen as  $N = 100$ .

It is clear from our formalism that the density profile should have the same kind of discontinuity that the Boltzmann factor of  $V(r)$  since  $\rho(r) = m(r)G(r;r)$  with  $m(r) = m \exp(-V(r))$  and  $G$  continuous at the interfaces. Actually this is a more general result of statistical mechanics of inhomogeneous fluids at discontinuous interfaces. In general for a fluid with density  $n(x)$  near a planar interface characterized by an external potential  $V_{\text{ext}}(x)$  eventually discontinuous at  $x = 0$  the  $y$ -function  $\exp(-V_{\text{ext}}(x))n(x)$  is continuous [23]. In region 2, the density far from the interfaces is close to the bulk value (4.16). In the borders, away from the interfaces the density tries to be close to the new bulk value given by Eq. (4.16) replacing  $m$  by  $m_0$ . If the width of the border region was much larger than  $m_0^{-1}$ , one would expect that the density far away from the interfaces converges to a bulk value according to the value of  $m(r)$  in that region.

In relation with this behavior we should clarify a delicate point. Since the individual densities of the particles are divergent, we had to cut off the sums in Eq. (4.47) to a maximum value of  $N$  equal to  $N = 100$  in the figures. The first term in the sum of Eq. (4.47) when  $r_1 = r_2 = r$  is the bulk density (4.16) and it is an (infinite) constant if all the terms in the sum are considered. However with a cutoff this term is not constant anymore. This artificially makes the density in the outer region 3 look smaller than in the inner region 1 in Figures 9 and 10.

Figure 10 shows the density profile of the positive particles. One can notice that the profile is continuous across the boundaries as expected since positive particles are not submitted to any discontinuous external potential. In region 2, away from the interfaces the density approaches the bulk value given by Eq. (4.16). In the border regions 1 and 3 away from the interface the density tries to stabilize to a new higher bulk value given by Eq. (4.16)

but replacing in that equation  $m$  by  $m_0$ . This is due to the natural tendency of the system to be electrically neutral. The positive particles try to follow the negative ones so the system is not locally charged. However at the interfaces  $r = R_1 + \delta$  and  $r = R_2 - \delta$  there remains a non-neutral charge density that can be seen in Figure 11. Actually one can see in Figure 11 a double charged layer. Inside the border region (1 or 3) there is a negative charge density layer and outside the border, in the bulk region 2, a positive layer, the same one that was previously observed with model I in Figure 7. These double layers are concentrated near the interfaces at  $r = R_1 + \delta$  and at  $r = R_2 - \delta$  and have a thickness of order  $m_0^{-1}$  for the positive layer in region 2 and  $m_0^{-1}$  for the negative layer in regions 1 and 3.

## V. SUMMARY AND PERSPECTIVES

The present solvable model studied here gave us interesting information about the behavior of confined Coulomb systems with attractive boundaries. This system has an induced internal charge on the boundary which is created by an external potential which is not of electrical nature. This potential only acts on the negative particles, while the positive particles are unaffected. This is not the usual situation that has been studied extensively in the past, where the system is submitted to electrical forces due to possible external charges.

First, we found that large systems exhibit the same finite-size corrections that for systems without attractive boundaries, confirming again the universal nature of these finite-size corrections. Studying the disjoining pressure we found that the attractive boundaries have a stabilizing effect. This was noticed also in our previous work [3], however the curvature in the present case is very important. It makes the surface tension to be the predominant contribution to the disjoining pressure, as opposed to the slab geometry. Then, we conclude that the curvature has also a stabilizing effect on the system in comparison to the slab geometry in which the system can be unstable for low values of the adhesivity.

The study of the density profiles gives information about the structure of the system. As expected, there are some absorbed charges on the boundary and these are screened by a positive layer of charge inside the system. We were able to check explicitly a few sum rules (electro-neutrality sum rule) and relations that the absorbed charge in the boundary satisfy.

It would be interesting to know what features of the present model are universal and which are not. A step toward answering this question can be obtained by studying another solvable model of Coulomb system, the one-component plasma. A preliminary study of this system was done in Ref. [15] and this will be the subject of a future paper.

## A cknow ledgm ents

The authors would like to thank the following agen-cies for their nancial support: ECO S-N ord (France),

CO L C IEN C IAS-IC FES-IC ET EX (Colombia), Banco de la R epublica (Colombia) and Fondo de Investigaciones de la Facultad de C iencias de la U niversidad de los A ndes (Colombia).

---

[1] M . L .R osinberg, J .L .Lebow itz and L .B lum , A Solvable M odel for Localized Adsorption in a Coulomb System , J . Stat . Phys . 44:153{182 (1986).

[2] F .Comu, Two-D imensionalM odes for an Electrode with Adsorption Sites, J . Stat . Phys . 54:681{706 (1989).

[3] G .T ellez and L .M erchan, SolvableM odel for Electrolytic Soap Film s: The Two-D imensional Two-C omponent P lasma, J . Stat . Phys . 108:495{525 (2002).

[4] L . Sam aj and I . T ravenec, Therm odynam ic P roperties of the Two-D imensional Two-C omponent P lasma, J . Stat . Phys . 101:713{730 (2000).

[5] L . Sam aj and B . Jancovici, Surface Tension of a MetalElectrolyte Boundary: Exactly Solvable M odel, J . Stat . Phys . 103:717{735 (2001).

[6] L . Sam aj, Surface Tension of an Ideal D ielectric-E lectrolyte Boundary: Exactly Solvable M odel, J . Stat . Phys . 103:737{752 (2001).

[7] M . G audin, L 'isotherme critique d'un plasma sur rseau ( $\epsilon = 2$ ,  $d = 2$ ,  $n = 2$ ), J . Physique (France) 46:1027{1042 (1985).

[8] F .Comu and B . Jancovici, On the Two-D imensional Coulomb G as, J . Stat . Phys . 49:33{56 (1987).

[9] F .Comu and B . Jancovici, The electrical double layer: A solvable m odel, J . Chem . Phys . 90:2444{2452 (1989).

[10] P . J .Forrester, D ensity and correlation functions for the two-com ponent plasma at  $\epsilon = 2$  near a metalwall, J . Chem . Phys . 95, 4545{4549 (1991).

[11] B . Jancovici, G .M aniaci and C .P isani, Coulomb System s Seen as CriticalSystem s: F inite-Size E ffects in Two D imensions, J . Stat . Phys . 76, 307{329 (1994).

[12] B . Jancovici and G . T ellez, Coulomb System s Seen as Critical System s: Ideal Conductor B oundaries, J . Stat . Phys . 82, 609{632 (1996).

[13] B . Jancovici and L . Sam aj Coulomb System s with Ideal D ielectric B oundaries: Free Ferm ion Point and Univer-sality, J . Stat . Phys . 104, 753{775 (2001).

[14] G . T ellez, Two-D imensional Coulomb System s in a Disk with IdealD ielectric B oundaries, J . Stat . Phys . 104, 945{970 (2001).

[15] L .M erchan, Two-dim ensionalC oulomb system s in a con- nected geom etry subject to an attractive potential on the boundary, M aster Thesis (U niversidad de los A ndes, B ogota, 2003).

[16] P . J .Forrester, Surface Tension for the Two-C omponent P lasma at  $\epsilon = 2$  near an Interface, J . Stat . Phys . 67:433{448 (1992).

[17] J .L . Cardy and I . Peschel, F inite-size dependence of the free energy in two-dim ensional critical system s, Nucl . Phys . B 300, [FS 22]:377{392 (1988).

[18] J .L . Cardy, in Fields, Strings and C riticalPhenomena, Les Houches 1988, E . B rezin and J . Z inn-Justin, eds. (North-Holland, Am sterdam , 1990).

[19] M . Abramow itz and I .A . Stegun, H andbook of M athe-m aticalFunctions (N ationalB ureau of Standards, W ashington, D .C ., 1964).

[20] E . H . H auge and P . C . H em m er, Phys . Norv . 5, 209 (1971).

[21] S .G radshteyn and I .M . R yzhik, Table of Integrals, Se-ries, and P roducts (Academ ic, N ew York, 1965).

[22] G .N .W atson, A treatise on the theory of Besselfunctions (Cam bridge U niversity P ress, U K , 1922).

[23] J .R .H enderson, in Fundamentals of inhom ogeneous u-ids, Chap . 2, D .H enderson, ed. (M .D ekker, N ew York, 1992).